

Light scattering by a liquid-gas helium spray^{*}

Y. Ladam, P.-E. Wolf, P. Thibault, and L. Puech^a

Centre de Recherches sur les Très Basses Températures, laboratoire associé à l'Université Joseph Fourier, CNRS, BP 166, 38042 Grenoble Cedex 9, France

Received: 31 July 2000 / Revised and Accepted: 7 December 2000

Abstract. Light scattering by liquid helium droplets or gaseous helium bubbles is strongly forward. This has two direct experimental consequences: rare scatterers are very bright in a narrow ($\ll 5^\circ$) angular region in the forward direction; and even in the presence of multiple scattering the intensity collected at large angles is linear in the concentration of scatterers. These properties are explained, and the second one is illustrated with a liquid-gas helium spray.

PACS. 87.57.Gg Image reconstruction and registration – 42.30.Wb Image reconstruction; tomography – 42.68.Jg Effects of aerosols

1 Introduction

We have recently developed an experiment for studying spray formation and evaporation, using a rapid annular flow of gaseous helium (GHe) to atomize a central, slower, circular jet of liquid helium (LHe) [1]. Varying the gas temperature allows to vary the evaporation rate of the spray, and to investigate the influence of this parameter on the spray by means of light scattering [2].

In the study of spray formation and flow, light scattering by particles (*e.g.* droplets) is an attracting mean of accessing particle size, density and/or velocity. It is essentially a non-intrusive and relatively local probe. In our case and others, light scattering is used to map out by direct imaging the concentration of scatterers, or more precisely, in our context of spray formation, the liquid-gas interface density. Generally, the validity of this method is however restricted to low density sprays, such that only single scattering occurs. At larger densities, due to multiple scattering, the scattered intensity is no longer a monotonous function of the scatterers concentration. Furthermore, the ability to establish a one-to-one correspondence between a point of an image and a given region of the spray is lost. Extracting information from such turbid media is the subject of recent intensive research.

The purpose of this paper is to stress that a specific situation arises for strong forward scattering, a case relevant in different contexts [3] as medicine, meteorology, astronomy, etc., . . . The case of helium is extreme in this respect: due to the very small contrast of optical index between gas and liquid helium ($\sim n - 1 = 0.02$), droplets larger than several microns in diameter scatter light at

very small angles ($\sim 5^\circ$). As we show below, this has two consequences. First, in the single scattering regime, the light scattered at such small angles is exceptionally large, allowing a sensitive detection of such droplets, even at minute densities. Second, even for a dense spray where strong multiple scattering occurs, the light scattered at much larger angles ($\theta \sim 45^\circ - 90^\circ$) can be used to image the spray.

This last point is illustrated in Figure 1 by two pictures of the same helium spray: as seen at 4° , and at 45° . At 4° , the denser region of the spray is darker than the surroundings, due to the fact that light is deflected at larger angles by strong multiple scattering. Still, the same region, when viewed at 45° , appears bright. For such a large angle, we shall show that the collected intensity remains linear in the density of scatterers, allowing a quantitative analysis.

2 CCD imaging of the spray in the single scattering regime

In our experiment, the light scattering analysis is quite simple: in a small solid angle (around scattering angles 4° , 45° , 90°), we capture a CCD picture of the illuminated portion of the spray, and perform a quantitative analysis of the intensity as function of position and of the relevant parameters.

In the single scattering regime, the intensity scattered in the direction Ω by a volume element $d^3\tau$, illuminated with the flux I_0 is:

$$\frac{dI}{d\Omega} = I_0 N \frac{d\sigma}{d\Omega} d^3\tau \quad (1)$$

where N is the particle density and $d\sigma/d\Omega$ the differential cross section. For a polydisperse spray, $Nd\sigma/d\Omega$

^{*} This paper has been presented at "Sixièmes journées de cryogénie et supraconductivité", 16–19 May 2000, Aussois.

^a e-mail: lpuech@labs.polycnrs-gre.fr

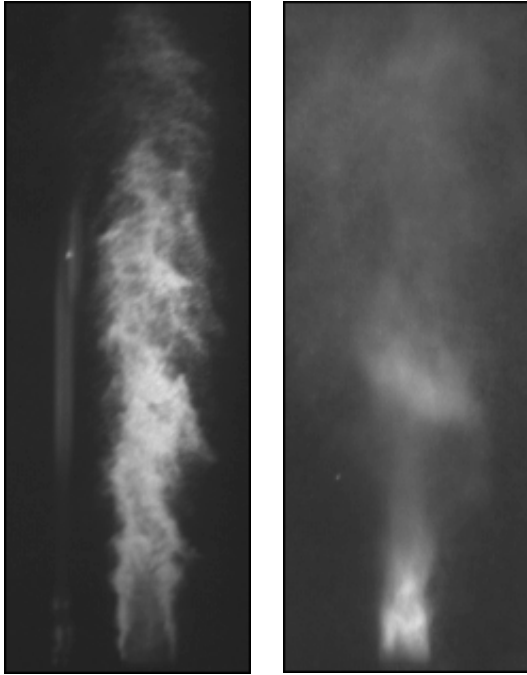


Fig. 1. The LHe/GHe spray in similar conditions, as seen -left as viewed at $\theta \sim 4^\circ$, -right at $\theta \sim 45^\circ$. Exposure times are different. Scale is approximately 1.5:1.

has to be understood as averaged over particle sizes. For spherical particles of radius r much larger than the wave length λ , the total scattering cross section is twice the geometrical cross section [4], geometrical optics (refraction plus reflexion) and diffraction each accounting for one half of the total. For particles larger than $20 \mu\text{m}$ in diameter (corresponding to a size factor $x = 2\pi r/\lambda$ of 100 at a wavelength of 632 nm), the contribution of diffraction is concentrated within a narrow angle around the forward direction ($\delta\theta \sim \lambda/2r \sim 2^\circ$). In the following, we consider the case of observation at larger angles, for which diffraction is negligible and the scattered light is controlled by geometrical optics only, so that $d\sigma/d\Omega$ is proportional to the particle surface $4\pi r^2$. Introducing the liquid-gas interfacial density $\Sigma = 4\pi r^2 N$ (with units of m^2/m^3), the scattered intensity is given by:

$$\frac{dI}{d\Omega} = I_0 \Sigma \left[\frac{d\sigma}{4\pi r^2 d\Omega} \right] d^3\tau \quad (2)$$

where the bracketted term does not depend on the particle size. In this limit of geometrical optics, imaging the spray under a given observation angle allows to measure the spatial dependence of Σ .

The angular distribution of the singly scattered light is proportional to the so-called ‘‘phase function’’ $\Phi_1(\Omega)$ [4]. $\Phi_1(\Omega)$ describes a single scattering event, with the normalisation rule $\int \frac{d\Omega}{4\pi} \Phi_1 = 1$. For statistically isotropic scatterers, Φ_1 depends only on the scattering angle θ . Quite generally, it is more practical to consider Φ_1 as a function of the cosine $u = \cos\theta$, because this variable is equally distributed over the unit sphere $d\Omega = 2\pi du$.

The precise angular dependence of $\Phi_1(u)$ depends on the particle shape. In the following, we shall consider two limiting cases: perfectly spherical and totally random shapes. The key results of the analysis given below do not depend on such microscopic details. Conversely, particle shapes will be hardly accessed by light scattering experiments.

3 The multiple scattering regime

The scattered intensity at a fixed angle cannot increase indefinitely as Σ increases, because it is limited by the isotropic redistribution of I_0 . Also, an image maps out the probability that a photon has its last scattering at a given place. In presence of multiple scattering, this can be very different from the scatterers distribution in space. As a consequence, the analysis of Section 2 could be expected to fail when the average number of scattering events light experiences before being detected is larger than one. The purpose of the following is to show that the validity of this conclusion depends on the degree of forward scattering.

Considering the propagation of a single photon, successive scattering events translate to a random walk on the unit sphere, with transition probability $\Phi_1(\mathbf{n}, \mathbf{n}')$ from direction \mathbf{n} to direction \mathbf{n}' . Hereafter, the initial point of the random walk will be taken as the north pole of the sphere. When the number p of scattering events increases, the initial distribution of light spreads onto the sphere in a computable way, which we describe in Section 4. The resulting distribution is called $\Phi_p(u)$ in the following.

For a small index contrast, $\Phi_1(\Omega)$ is concentrated in the forward direction. This can be characterized by the average $\langle u \rangle_\Phi = 0.9959$ for liquid He spheres, in the regime of geometrical optics. This can be interpreted as giving an angular width $\sqrt{\langle \theta^2 \rangle} \sim 5^\circ$, although the concept of r.m.s. angle is not really relevant to the present situation, (see Sect. 4). In this case, many scattering events are needed to isotropize initially collimated light.

Depending on the shape of the angular distribution Φ_1 , two distinct behaviours can arise: either (case (i)) the random walk amounts to a normal diffusion around the pole of the sphere, or (case (ii)) the walk allows some rare large angular changes in a single step. In that second case, these large steps can control the intensity at a fixed (large) angle.

- Case (i) necessarily gives for large p a Gaussian distribution of light around the north pole:

$$\Phi_p(u) = \frac{1}{p2\pi\langle\theta^2\rangle_1} \exp\left(-\frac{\theta^2}{2p\langle\theta^2\rangle_1}\right) \quad (3)$$

i.e. $\langle\theta^2\rangle_p = p\langle\theta^2\rangle_1$. From this expression, it is obvious that the intensity at some finite angle is not linear in p , *i.e.* the proportionality to the particle concentration will break down in the multiple scattering regime.

- Case (ii) bears a very strong analogy with Levy flights [5] in a plane. For a fixed small angular width of Φ_1 (*i.e.* $1 - \langle u \rangle \ll 1$), if the shape of $\Phi_1(\Omega)$ is such

that the probability of large scattering angles is sufficient for exceeding the diffuse part of case (i), the intensity at that angle may increase linearly with p in some range for p . As an illustration of this fact, let us consider the phase function proposed by Henyey-Greenstein (H-G) [6]. Its shape has marked “wings” at large angle:

$$\Phi_1(v, u) = \frac{(1 - v^2)}{(1 + v^2 - 2uv)^{3/2}}, \quad (4)$$

in which $v = \langle u \rangle = \langle \cos \theta \rangle$ is the only parameter. The case $v = 0$ is isotropic scattering, and $v = 1$ is fully forward.

For small angular width and scattered angles (*i.e.* $\epsilon = 1 - v \ll 1$, $\delta = 1 - u \ll 1$) equation (4) reduces to $\Phi_1(v, u) = 2\epsilon/(2\delta + \epsilon^2)^{3/2}$, closely similar to a 2D Lorentzian distribution around the pole (recall that $\delta \sim \theta^2/2$ essentially measures the square of the distance to the pole). The characteristic width (FWHM) of such a distribution is $\delta^* \sim \epsilon^2$, which is much smaller than the average value over all angles $\langle \delta \rangle = \epsilon$ (since $\langle u \rangle = v$). In this sense, we may say that the “wings” of the H-G phase function are exceptionally probable.

We shall show in Section 4 that, after p scattering events, the phase function Φ_p retains the same H-G functional form, with a larger width given by $v_p = v^p$, thus implying $\epsilon_p \sim p\epsilon$. This means that the θ -FWHM scales as p , rather than $(p)^{1/2}$ for the Gaussian case.

Provided the angle of observation is large and the total number of scattering events not too large (namely for $1 > \delta \gg (p\epsilon)^2$ and $1 \gg p\epsilon$), one deduces from the above $\Phi_p \sim 2p\epsilon/(2\delta)^{3/2}$, proving that the scattered intensity is linear in p , in strong contrast with case (i). For LHe/GHe spray, we have $\epsilon \sim 1/250$. If the H-G function properly represents the true phase function, this linear behaviour will hold up to $p \sim 250$ scattering events.

In this range of multiple scattering, the light propagation to some “large” angle might be typically thought of as a large angle single scattering event separating two almost straight propagation paths consisting in a large number of small angle orientation changes. The scattered intensity is controlled by this large angle event, so that we have an effectively single scattering situation. In this regime, the interfacial density can be imaged by viewing the spray at a large scattering angle, as is the case in Figure 1. In contrast, in case (i), a large angle event typically arises by successive accumulation of much smaller deviations, and the ability of retrieving the interfacial density is lost.

The distinction between cases (i) (Gaussian scattering), and (ii) (non Gaussian scattering), has been already made in [7]. In this reference, similar conclusions are drawn concerning the Lorentzian character of the H-G phase functions, and the irrelevance of the concept of r.m.s. scattering angle in that case. However, the consequences on the intensity scattered at large angles were not discussed in this reference.

4 Convolution on the sphere, Legendre polynomials

Successive scattering events with the same Φ_1 yields the recursion equation for the angular distribution after p scattering events:

$$\Phi_{p+1}(\mathbf{n}) = \int \frac{du'}{2} \frac{d\phi'}{2\pi} \Phi_1(\mathbf{n}, \mathbf{n}') \Phi_p(\mathbf{n}'). \quad (5)$$

We stress that, unlike the radiative transfer equation [8], the exact¹ equation (5) does not convey any information on the location of the successive scattering events. The counterpart is that it can be exactly solved by expanding the Φ 's on Legendre polynomials with coefficients ${}^{(p)}\nu_\ell$:

$$\Phi_p(u) = \sum_{\ell} {}^{(p)}\nu_\ell (2\ell + 1) P_\ell(u) \quad (6a)$$

with

$${}^{(p)}\nu_\ell = \langle P_\ell(u) \Phi_p(u) \rangle_u. \quad (6b)$$

Making use of orthogonality rules, it can be shown that:

$${}^{(p+1)}\nu_\ell = {}^{(1)}\nu_\ell {}^{(p)}\nu_\ell. \quad (7)$$

Thus, using the Legendre polynomials, the convolution like expression (5) transforms to a simple product (7), very much like the Fourier transform turns a convolution into a simple product. For the particular case of the H-G function we have [8] ${}^{(1)}\nu_\ell = v^\ell$. This property implies that, after p scattering events, Φ_p retains its H-G form with $\langle u \rangle_p = v^p$ as used in Section 3.

In the next section, we will make use of a modified H-G function having for large ℓ , and small $1 - v$: ${}^{(1)}\nu_\ell = v^{\ell^\alpha}$ with $1 \leq \alpha \leq 2$, and $v = \langle u \rangle$. This set of new phase functions includes the H-G (case (ii), $\alpha = 1$) and the Gaussian² (case (i), $\alpha = 2$) functions, and allows some adjustment to the expected true phase function. This set is also stable under the convolution (5), at fixed α .

In practice, we are interested by the light emerging from the sample, *i.e.* for which the last scattering event is within a scattering mean free path l from the sample boundary. Due to this constraint, the resulting angular dependence generally bears no similarity to $\Phi_p(u)$. The case of strong forward scattering is an exception in this respect. For a slab thickness L , such that $l \ll L \ll l/\epsilon$, the light transmitted through the sample remains partially collimated, and the transmitted intensity will be dominated by scattering paths all having the length L in real space. For such paths, p is a random variable obeying the Poisson distribution $P_t(p) = t^p e^{-t}/p!$, with a given average number of scattering events, $\langle p \rangle = t = L/l$.

¹ Insofar as random interferences between different scattering sequences are neglected.

² The true Gaussian phase function can be shown to satisfy $\nu_\ell = v^{\ell(\ell+1)/2}$, yielding $\alpha = 2$ at large l , *i.e.* for strongly forward scattering.

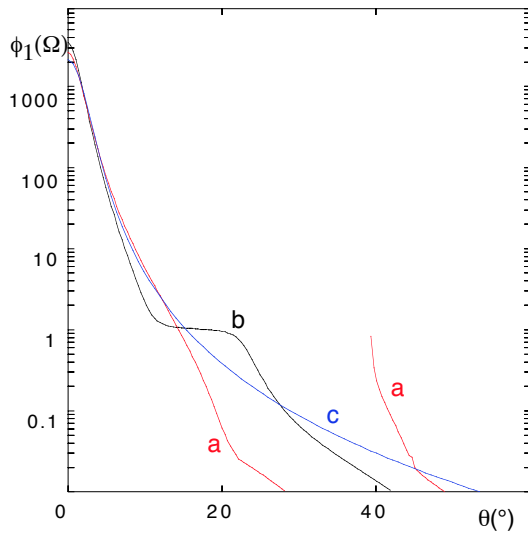


Fig. 2. The phase function $\Phi_1(\Omega)$ plotted *versus* $\theta(^{\circ})$. (a) As calculated for a spherical drop, (b) for random orientations of interfaces, (c) interpolated function with simple Legendre expansion for (a) and (b), the Snell-Descartes reflection coefficients were evaluated and averaged over polarization of light. Note the very strong weight to the small angle region. The singularity in curve (a) at 40 is the “rainbow” described in the text.

The angular dependence of the transmitted light will then be approximately given by the exact average phase function $\Phi_t(u)$ for a given length $L = tl$, the coefficients of which ν_ℓ are found by averaging the coefficients ν_ℓ given by equation (7) over the distribution $P_t(p)$, yielding

$$\nu_\ell(t) = \nu_\ell(0) \exp\left(-t(1 - \langle \cos \theta \rangle_{\Phi_1}) \nu_\ell\right), \quad (8)$$

$\langle \cos \theta \rangle_{\Phi_1}$ being given by inserting $\Phi_1(u)$ in (6b).

Equation (8) shows that each “mode” ℓ has its characteristic decay time $t_\ell^* = 1/(1 - \langle \cos \theta \rangle_{\Phi_1}) \nu_\ell$. The energy flux in the incident direction solely involves the term $\ell = 1$, and decays within $t_1^* = 1/(1 - \langle \cos \theta \rangle_{\Phi_1})$ collisions, a well-known result [8] (t_1^* is the ratio of the so-called transport and scattering mean free paths). In realistic cases t_1^* is the longest of the t_ℓ^* s, and is an order of magnitude of the number of collisions necessary to isotropize the energy flux. It is about $t^* = 250$ for the LHe/GHe system.

We have now a general scheme for evaluating $\Phi_t(u)$ for arbitrary Φ_1 : calculate the $\{\langle \cos \theta \rangle_{\Phi_1}\}$ with (6b), insert in (8), calculate $\Phi_t(u)$ by resummation of (6a). Of course the calculation is truncated to some ℓ .

5 Explicit calculation for LHe drops

In Figure 2, the phase function is shown as function of θ for $n = 1.02$ for three models droplets³:

³ Hereafter, we consider only geometrical optics and neglect the influence of diffraction. This is justified for large enough particles for the diffraction angle to be much smaller than 5° .

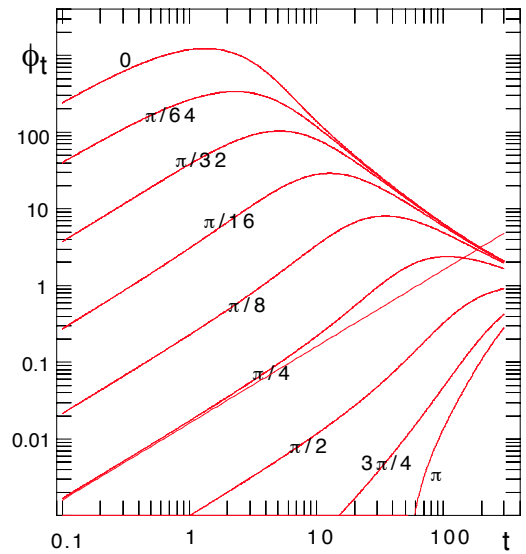


Fig. 3. The intensity collected as a function of average number of collisions, for several characteristic angles. Calculation used equation (8) and curve (c) of Figure 2. The straight line is the extrapolation of the single scattering regime for $\theta = \pi/4$.

- (a) Spherical drop, taking into account direct refraction, and at most one reflection. The higher order terms (two or more reflections) yield very small changes since they involve higher powers of $(n - 1)^2$. The light reflected inside the droplet has a minimal deviation of about 40° (for water drops, the same minimal deviation is close to 150° and, combined with dispersion, is the origin of the rainbow).
- (b) Light impinges on some gas-liquid interface of random orientation, and is either reflected or transmitted. If transmitted, it then impinges on successive liquid-gas interfaces of random orientation, until it is finally transmitted. This apparently complicated situation can be calculated using the factorisation of Section 4. Curves (a) and (b) are very similar, except near the “rainbow” feature at 40° , which indeed relies on perfectly spherical shape of drops, which are not expected in typical experiments.
- (c) A modified H-G function with $\langle \cos \theta \rangle_{\Phi_1} = v^{\ell^\alpha}$ with $v = 0.99593$ and $\alpha = 1.44$, chosen to interpolate smoothly between (a) and (b).

In Figure 3, the intensity computed according to the scheme discussed in Section 4, using the phase function (c), is plotted *versus* the average number of scattering events, t , for some typical angles. It is obvious from this figure that the total intensity at 45° or 90° scales like t for $t < 100$, within a factor 2. This means that we are in case (ii) of Section 3, with 45° or 90° large enough for the scattering to be effectively single at these angles (*i.e.* the angular deviation is obtained by only one scattering event at large angle). The total light collected at such large angles is then proportional to the integral of Σ over the incident path within this factor of two accuracy.

Furthermore, as discussed at the end of Section 3, Σ can be imaged in this regime. This fact has been extensively used in reference [2]. In contrast, at small angles and in the same range of t values, Figure 3 shows that the angular distribution of the scattered light is progressively widened by the multiple scattering. As discussed in Section 4, this evolution directly controls the angular distribution of the transmitted light when the slab thickness L is smaller than some tens of scattering mean free paths (*i.e.* t smaller than some tens). Measuring this distribution provides a second way to access t , *i.e.* l , or, equivalently in the regime of geometrical optics, Σ , in the multiple scattering regime, with results consistent with those obtained from the large angle scattering [2].

6 Conclusion

The small index contrast between gas and liquid He produces a phase function which is strongly peaked in the forward direction. This has the consequence that in the single scattering regime, the light is extremely intense in the small angle region ($\theta < 5^\circ$). This fact shows that collimated light and small angles must be used for detecting rare He drops or bubbles.

At large angles, the signal can be quite small compared to more conventional scatterers, but remains linear with the average number of scattering events t , even in the strongly multiple scattering domain $t \sim 100$. This fact

allows quantitative estimates of interfacial density Σ , even in dense regions of a LHe/GHe spray, provided t remains less than about 100.

We are grateful to B. Van Tiggelen for pointing out reference [7], and to B. Castaing for his suggestions. This work was performed under contract with Société Européenne de Propulsion, and financially funded by CNES/CNRS through the "Groupement de Recherches sur la Combustion dans les Moteurs de Fusées".

References

1. Y. Ladam, P.E. Wolf, L. Puech, *2nd Int. Symposium on Heat and Mass Transfert* (Delft University Press, 1997).
2. Y. Ladam, Thesis at Université Joseph Fourier, March 2000.
3. G.W. Kattawar, H.C. Van de Hulst, *Appl. Opt.* **33**, 5820 (1994).
4. H.C. Van de Hulst, *Light Scattering by small particles* (Wiley, New York, 1957. Dover paperback reprint, 1981).
5. J.P. Bouchaud, in *Levy Flights and Related Topics in Physics*, *Proceedings of the International Workshop* (Springer-Verlag, Berlin, 1995).
6. L.G. Henyey, J.L. Greenstein, *Astrophys. J.* **93**, 70 (1941).
7. H.C. Van de Hulst, *Reviews in Modern Astronomy*, edited by R.E. Schielicke, 1996, Vol. 9.
8. H.C. Van de Hulst, *Multiple Light Scattering* (Academic Press, 1980), Vol. 2, p. 308.